ORIGINAL PAPER

Microfibrillated Cellulose-Silver Nanocomposite Based PVA Hydrogels and Their Enhanced Physical, Mechanical and Antibacterial Properties

Md. Sabbir Hasan[1,2] · Jannat Al Foisal[1,4] · G. M. Arifuzzaman Khan[1] · Rownok Jahan[1] · Md. Hasanuzzaman[1,6] ·
Md. Shamsul Alam[1] ⓘ · M. Minnatul Karim[3] · M. A. Gafur[5] · Muhammad Angkan Khan[3] · Md. Abdus Sabur[3]

Abstract

Modification of cellulose with silver nanoparticles produces various nanocomposites with significantly developed properties. This work aims to prepare a PVA hydrogel modified with cellulose/silver nanocomposites having potential applications in various fields including biomedical, antimicrobial inhibition, textile wears, etc. Microfibrillated cellulose/silver nanocomposites hydrogels were prepared in the aqueous medium with aid of microwave-assisted heating. Different percentages of nanocomposites were incorporated in PVA hydrogel to enhance the properties of PVA hydrogel. Prepared products were characterized by UV–Visible spectroscopy, FTIR, TGA, XRD, and SEM. The swelling (in water saline, acidic and alkaline solution), tensile, thermal, and antibacterial properties were also examined. The formation of Ag nanoparticles (AgNPs) in the (MFC-Ag)NC was confirmed by XRD and UV–Vis spectra. UV–Vis spectra showed the characteristic peaks of Ag in the UV–Vis spectra at 425 nm. Final products exhibited significant porosity and maximum swelling of 519.44%. The thermal stability of hydrogel increased with an increased percentage of (MFC-Ag)NC. Hydrogels exhibited significant antimicrobial inhibition against multidrug-resistant microorganisms, including *Escherichia coli*, *Staphylococcus aureus*, and *Pseudomonas aeruginosa*.

Graphical Abstract
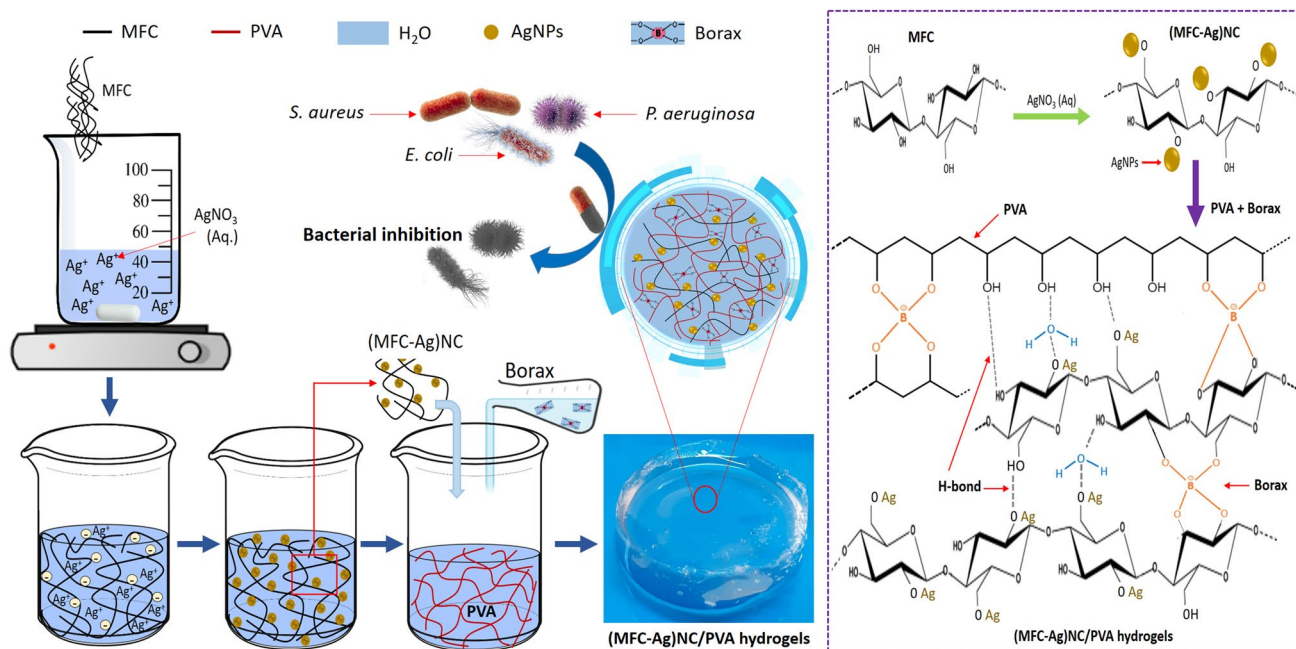
Extended author information available on the last page of the article

Introduction

Due to the unique physical properties hydrogels is an attractive material being used in the various field starting from biomedical, adsorption, textiles, etc. Very low adverse effects to cells and tissues, high water content, and biocompatibility of hydrogels making it a suitable material for applications in the biomedical field including drug delivery systems, biomedical devices, tissue engineering, contact lenses, hygiene products, etc. [1–7]. Among different prerequisite biocompatibility and nontoxicity with the substrate to which hydrogels are applied is a major concern for the hydrogel intended for biomedical applications [8]. Due to the presence of hydroxyl group polyvinyl alcohol (PVA) shows strong hydrophilicity. Hydrophilic nature and some desired characteristics of PVA including good self-healing capability, biocompatibility, and nontoxicity make it suitable in the field of biomedical [8–10]. The presence of the hydroxyl group makes PVA reactive and can be functionalized to form hydrogels by chemical and physical means of crosslinking with many types of functional groups. Physical crosslinking through hydrogen bonds is a common technique for PVA hydrogels synthesis. Borax has been successfully used as a chemical crosslinking agent for PVA. Borax produces borate ions in the aqueous medium and crosslinked chemically with PVA with the formation of extensive hydrogen bonds remarkably increase the viscoelasticity of the PVA in aqueous solutions which leads to the formation of hydrogel's 3D bridge network. Borax produces borate ions in aqueous medium form complexes with hydroxyl groups of PVA that act as a temporary cross-linker [11–14]. Numerous studies have been revealed that composites of PVA hydrogels can be prepared with different compounds including sodium alginate, hyaluronan (HA), modified montmorillonite clay, AgNPs, cellulose nanocrystals (CNC), microcrystalline cellulose (MCC), cellulose fibers (CF), holocellulose (HC), gum acacia, bacterial cellulose (BC), MFC, and chitosan [15–19]. The resulting PVA hydrogels incorporated with nanocellulose or silver nanoparticles exhibited desirable properties for biomedical applications [20, 21].

Cellulose, the most abundant, sustainable, and environment-friendly natural polymer attracts much attention in biomedical applications due to its excellent biocompatibility. The nanostructured cellulose such as nanocellulose (NC), cellulose nanocrystal, microfibrillated cellulose (MFC) acts as a potential aspirant in hydrogels because of its affluence, high stiffness, low toxicity, and low weight [22, 23]. Extensive hydrogen bonding can create interconnected networks throughout cellulose structure via crosslinking to form hydrogels [24]. The use of these nanofibers in hydrogel has proven effective due to the large surface area and enhanced mechanical properties presented by cellulose [25]. Since cellulose itself rarely possess antibacterial properties, cellulose/PVA hydrogels are not efficient in therapeutic purposes. AgNPs have been widely used as topical antibacterial agents with luscious antimicrobial activity and fewer side effects to minimize the abuse of broad-spectrum antibiotics [26]. Instead of cellulose, Cellulose-Ag nanocomposites can exert significant antimicrobial activity and demonstrate variant applications in the public health sector and biomedical field [27, 28]. Cellulose incorporated with AgNPs lead to the formation of (MFC-Ag)NC which can be utilized extensively because of a wide range of properties subsuming high mechanical strength, biodegradation, bio suitability, and stability against a variety of chemicals [18]. It has also been reported that the incorporation of (MFC-Ag)NC into PVA improved the antimicrobial properties as well as mechanical properties as compared to individual MFC and AgNPs due to the synergistic effects between both nanomaterials [29].

Commonly, AgNPs are synthesized by the reduction of silver compounds by different techniques. A chemical stabilizer is needed to protect the nanoparticles from clustering. Fortunately, cellulose can act as both reducing and stabilizing agents. However, the main problem of synthesizing AgNPs is the consistency to get uniform properties namely morphology, chemical reactivity, crystalline structure, etc. The properties of AgNPs are mostly dependent on the synthesis method. In the present study, AgNPs have been prepared microwave-assisted. It is expected that cellulose molecules might create sufficient reactive cite under microwave heating which can increase the reduction of silver to produce more nanosilver and form (MFC-Ag) nanocomposite. The nanocomposites have been incorporated in PVA hydrogels to enhance the physical and mechanical properties of hydrogels. Besides this, the MFC-Ag nanocomposite can be generated the crosslinking network with PVA by hydrogen bonding without minimum reduction of swelling capacity because MFC acts as a superabsorbent. The thermal properties of cross-linked (MFC-Ag) nanocomposite/PVA hydrogels have not been reported in the literature before. Therefore, we have investigated the thermal properties of hydrogels to understand the effect of (MFC-Ag)NC. The previous studies have been suggested that the cellulose-AgNP incorporated PVA hydrogel is effective for *Escherichia coli* and *Staphylococcus aureus* [20, 30, 31]. Like *E. coli* and *S. aureus*, *Pseudomonas aeruginosa* caused harmful effects in the tropical area and it became resistant to multiple drugs. However, no work has been found on the usefulness
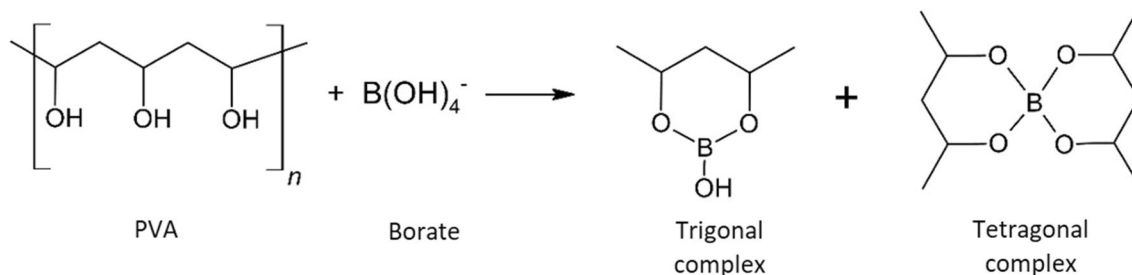
Scheme 1 Reactions between PVA and Borax

of cellulose-AgNP incorporated PVA hydrogel against *P. aeruginosa*. In this study, we have considered the antibacterial activity of synthesized hydrogels against *E. coli* and *S. aureus*, and *P. aeruginosa* bacteria. All bacteria used in this study were multidrug-resistant reported [32].

Experimental

Materials

Textile wastage was collected from Ha-Meem Group Garment Industries Ltd. Dhaka, Bangladesh which was transformed into cotton linter for the experiments. Borax was collected from the local market and purified by recrystallization method to remove sand, dirt, etc. Silver nitrate anhydrous (extra pure) and PVA were brought from MolyChem, India, and LobaChemie, India respectively. Other analytical grade chemicals such as sodium hydroxide (> 97%), glacial acetic acid (99.7%), sodium chlorite (80%), sodium metabisulfite (97%), sulphuric acid (> 98%), silver nitrate (> 99%) and acetone (> 98%) (all were purchased from Merck, Germany) were used without further purification.

Methods

Preparation of Microfibrillated Cellulose

Cotton linter can be used as an alternating source of α-cellulose as this is a cheap by-product of various garments industries in Bangladesh. MFC was prepared from cotton linter by several steps [33]. Sodium lauryl sulfate (5%) was used to wash cotton linter in the water bath at 40 °C for 30 min followed by subsequent drying for 8 h under vacuum at 60 °C after rinsing with distilled water. Dried cotton linter was treated with alkali and was bleached to remove the impurities and to extract pure α-cellulose using the conventional methods [33–35]. MFC was prepared by acid hydrolysis of extracted α-cellulose by the method mentioned in the previous work [36–38].

Synthesis of MFC-Ag Nanocomposites

(MFC-Ag)NC was synthesized by microwave-assisted heating with a very simple experimental setup. 0.481 g MFC and 0.403 g $AgNO_3$ were placed in a 100 ml beaker. 50 ml deionized water was added to it and stirred for 2 h with a magnetic stirrer to form a suspension. The beaker was sealed carefully with aluminum foil before placing it in the microwave oven (Memmert, Germany, Models -UF with forced air circulation, from 30 °C to 220 °C) to avoid expelling of acid vapor and was heated for 15 min at 150 °C. After heating, the suspension was allowed to cool at room temperature. (MFC-Ag)NCs were separated from the dark brown suspension using successive centrifugation. The (MFC-Ag)NCs were washed with water several times until acidity was removed completely. Finally, the nanocomposite was washed with acetone and dried under a vacuum at 60 ℃.

Preparation of (MFC-Ag)NC /PVA Hydrogels

The hydrogel was prepared using borax, PVA, and (MFC-Ag)NC as key ingredients. A certain amount of PVA was dissolved in distilled water at 85 °C. The pre-calculated amount of (MFC-Ag)NC was dispersed in a little amount of hot water and immediately added into the PVA solution. The (MFC-Ag)NC The borax was used as a cross-linker and the solution was added to this dispersed mixture. Borate ions get attached to the PVA molecules to form trigonal and tetrahedral 'di-diol' structures [39]. Although the mixture became viscous after adding borax, the transparent hydrogel was formed within a minute. The hydrogel was cured at 80 °C for 24 h. To investigate the effect of nanocomposite on hydrogel, the samples were prepared with 0 wt%, 0.5 wt%, 1 wt%, 2 wt%, and 5 wt% of (MFC-Ag)NC (Scheme 1, Fig. 1).

Characterization

UV–Vis absorption spectra of MFC and (MFC-Ag)NC were examined by Shimadzu UV-1600 spectrophotometer from 190 to 800 nm. The infrared spectra (scanning range 4000–700 cm^{-1}) of MFC, (MFC-Ag)NC and hydrogels were

Fig. 1 (MFC-Ag)NC/PVA hydrogels **a** prepared in beakers and **b** formed hydrogel
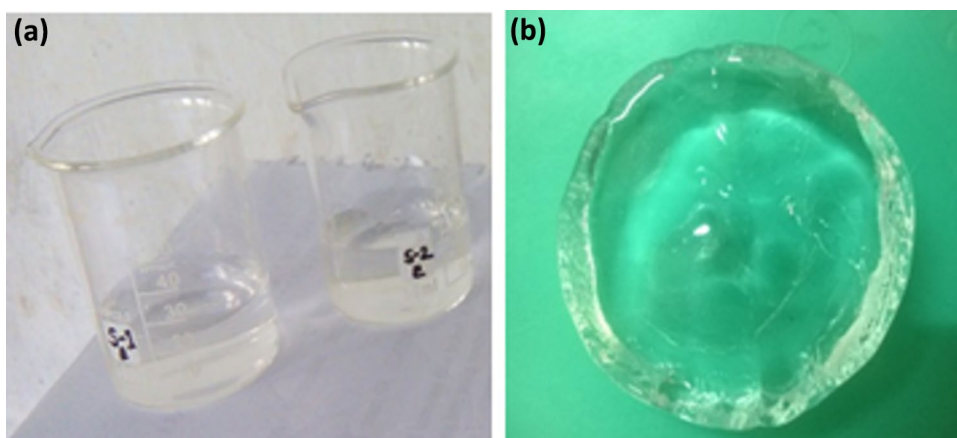
recorded with FTIR (8400S, Shimadzu, Japan) spectrophotometer. The diffraction pattern and crystallographic structure of MFC and (MFC-Ag)NC were examined using an XRD diffractometer (D8-Advance, Bruker, Germany) from 5° to 70°. Sample composition and surface topography were examined with a scanning electron microscope (JSM-7610F, JEOL Co. Ltd., Japan). To investigate the thermo-analytical response and thermal stability of the materials, Extrar 6300 TG/DTA, Seiko, Japan was used. The process was carried out under the inert environment of nitrogen gas with a scanning rate of 20 °C/min. The detection range was set from room temperature to 600 °C.

Swelling Test

The hydrogel samples were weighed and then submerged in distilled water at room temperature. The weights of specimens were taken at an interval of 24 h after wiping with a tissue to remove the excess water. The degree of swelling was measured till 72 h by the following equation: [39]

$$Swelling\% \; (Pure \; water) = \frac{Ws - Wd}{Wd} \times 100$$

where Ws = the weight of the gel in the swollen state and Wd = the weight of the gel in the dry state.

The swelling tests were also performed in saline water (0.9% NaCl), pH 1, pH 4, pH 10, and pH 13. All reported values are the average of three experiments.

Tensile Strength Test

Tensile strength test of hydrogels was performed at room temperature using a 60kn WDW-S series Hounsfield tensile testing machine (China). The dimension of test samples was $4 \times 40 \times 6$ mm^3. The conditions were set as follows: Crosshead speed of 2 mm/min and a gauge length of 20 mm. The initial cross-section of 40 mm^2 was used for calculating the tensile stress and Young's moduli.

Antimicrobial Activity

The well diffusion method was used to test the antibacterial activity of prepared (MFC-Ag)NC/PVA hydrogels according to the guideline of the National Committee for Clinical Laboratory Standards (NCCLS) [40]–[42]. The gram-negative *Escherichia coli* MZ20 and *Pseudomonas aeruginosa* MZ2F and gram-positive *Staphylococcus aureus* MZ18 were grown in Luria–Bertani (LB) for 18–20 h. The bacterial inoculums were prepared by maintaining turbidity of 0.5 McFarland standard (equal to 1.5×10^8 colony-forming units (CFU)/ml). Mueller Hinton agar (MHA) plates (150-mm diameter) were prepared, and bacterial suspensions were spread over the surface. Negative & positive bacterial strains of 100 µL each were placed on the solid culture medium. With the aid of a sterile tip, holes of a diameter of 8 mm were shoved and poured with (MFC-Ag)NC/PVA hydrogels with different concentrations of (MFC-Ag)NC. After pouring samples, the medium was kept at 37 °C for 24 h. The zone of inhibition for different strains was observed and measured after incubation.

Result and Discussion

Characterization of MFC, (MFC-Ag)NC, and (MFC-Ag)NC/PVA hydrogels

The absorbance spectra of MFC and (MFC-Ag)NC are shown in Fig. 2 measured by UV–vis spectroscopy. The spectra of (MFC-Ag)NC exhibited a strong absorbance band at 425 nm while there was no characteristic peak for MFC. The appearance of the peak at 425 nm is probably due to the surface plasmon excitation vibration effect of AgNPs which is following the previous studies [42]–[44]. It has also been observed that the UV absorption band is positioned at a long-wavelength range between 350 and 500 nm. The position and intensity of the absorption peak of silver NP
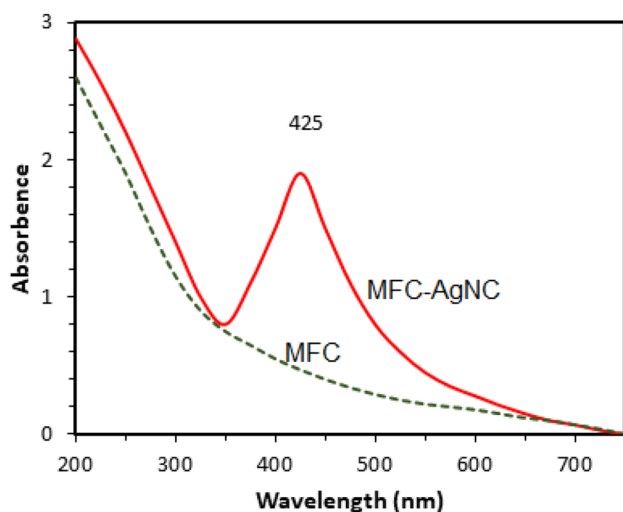
Fig. 2 UV–Vis absorption spectra

may be depended on its size, shape, and surface capping agents [43]. Gu-Joong Kwon et al. have revealed that the spherical AgNPs can absorb light within the wavelength range of 400–430 nm [45]. They also mentioned that nanocellulose can act as both template and the capping agents of the (MFC-Ag)NPs. Ag-NPs are formed by the reduction of Ag$^+$ ions by hydroxyl groups of cellulose followed by redox reaction by which metallic Ag is fixed within the cellulose porous structure.

Figure 3 shows the XRD pattern of MFC and (MFC-Ag)NC. The typical diffraction peaks assigned to cellulose and face-centered cubic (FCC) silver nanoparticles were observed clearly. The diffraction peaks at around
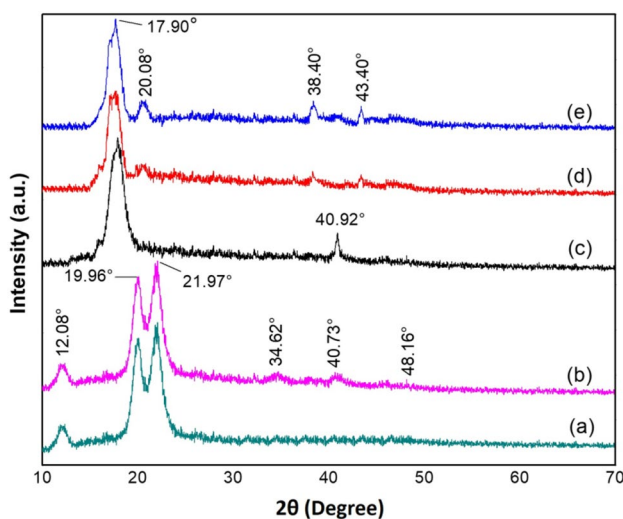
$2\theta = 12.08°$, $19.96°$, and $22.08°$ were observed due to the 101, 10 $\bar{1}$, and 002 planes of cellulose respectively. The peaks at around $2\theta = 34.74°$, $40.62°$, and $48.16°$ for (MFC-Ag)NC were noticed due to the well-crystallized silver nanoparticles with FCC structure [43]. It indicated that Ag$^+$ has been successfully reduced with the cellulose matrix under microwave-assisted heating and formed a crystalline structure. However, the intensity of the peaks at $34.74°$, $40.62°$, and $48.16°$ is smaller compared to identified peaks of cellulose at position $19.96°$, and $22.08°$.

Figure 4 shows the FTIR spectra of (MFC-Ag)NC, PVA, and PVA/(MFC-Ag)NC hydrogels. The (MFC-Ag)NC displays the typical bands of cellulose [46, 47]. In general, the absorption bands of (MFC-Ag)NC at around 3383 cm^{-1} is attributed to the stretching vibration of the hydroxyl group; 2897, 1666, 1487, 1028, and 833 cm^{-1} peaks correspond to the C–H group, C=O stretching in cellulose, C–H bending mode, C–O–C stretching mode from the glucosidic units [46], and C–H rocking vibration of cellulose [48] respectively. The characteristic absorption bands of PVA hydrogel are found at 3358 cm^{-1} which is corresponded to the O–H stretching of the hydroxyl group of the PVA; sharp band at 1649 cm^{-1} is assigned to the C-O stretching of the acetate group, and 1492 cm^{-1} is attributed to combination frequencies of (CH-OH) of PVA. The peak at 1427 cm^{-1} represents the trigonal complex structure between PVA and borate [49], which means the formation of trigonal structure is dominant in this hydrogel. No remarkable changes were observed on the spectra of PVA/ (MFC-Ag)NC hydrogels compared to the PVA hydrogel. The characteristics bands of MFC and PVA are closer to each other. Probably, in the hydrogels, the individual bands of MFC and PVA were overlapped.
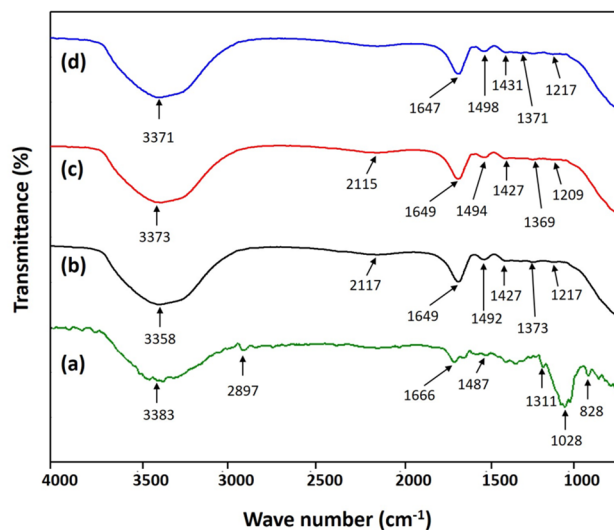

Fig. 3 XRD diffractogram of **a** MFC **b** (MFC-Ag)NC **c** PVA hydrogel **d** PVA/(MFC-Ag)NC (2wt%) hydrogel **e** PVA/(MFC-Ag)NC (5wt%) hydrogel


Fig. 4 FTIR spectrum of **a** (MFC-Ag)NC **b** PVA hydrogel **c** PVA/ (MFC-Ag)NC (2wt%) hydrogel **d** PVA/(MFC-Ag)NC (5wt%) hydrogel

Scanning electron microscopy (SEM) provides major information about the surface morphology of hydrogels. Figure 5 exhibits the surface morphology of (MFC-Ag) NC (a and b), pure PVA (c), and PVA/(MFC-Ag)NC (d) hydrogel samples following water removal by freeze drying. The images of (MFC-Ag)NC showed that the prepared composite was in the micro range, exhibiting the diameter of the composite materials as 0.07, 0.12, 0.15, 0.17 μm. After the removal of water, the voids formed inside the pure PVA hydrogel was circular or oval in shape and exhibited a diameter of 5–7 μm. The addition of (MFC-Ag)NC has brought substantial differences to the hydrogels, particularly in terms of the diameter of the void which decreased to 1–2 μm. As the amount of (MFC-Ag)NC was increased the distance between PVA chain reduced which in turn lead to a dense and relatively compact structure. Furthermore, a random void structure was observed compared to the circular and oval structure of pure PVA hydrogel. That's because of the random distribution of the (MFC-Ag)NC composite throughout the hydrogel structure.

Swelling Properties

Figure 6 shows the change of degree of swelling (DS) with time in distilled water, saline water, and various pH solutions. It has been seen that the swelling percentage of hydrogel is decreased with the increase of (MFC-Ag)NC loading (Fig. 6a). From the SEM it is seen that the pore size decrease with the addition of (MFC-Ag)NC. As hydrogels retain water into their structure with the help of their beehive structure. As the pore size decreases, it affects the swelling property. So it can be said that with a higher percentage of (MFC-Ag)NC incorporation, the pore size decreases which led to the decrease of swelling of hydrogels [50]. The maximum swelling percentage was found to be 519.44% for 0 wt% (MFC-Ag)NC. The addition of (MFC-Ag)NC till 1 wt% kept the swelling behavior similar to the maximum swelling was found at 48 h but after this period the degree of swelling tends to reduce. This could be due to the disintegration of the hydrogel. Whenever polymer molecules are swelled in a particular solvent, the physical bonds between the molecules become weak [51]. Therefore, the PVA hydrogel started to disintegrate after a complete swell in distilled water. This also suggests that the bonding was weak and the cross-linking of the hydrogel was physical bonding.

Fig. 5 FESEM images of (**a**) and (**b**) (MFC-Ag)NC (**c**) PVA hydrogel and **d** PVA/(MFC-Ag) NC (5wt%) hydrogel
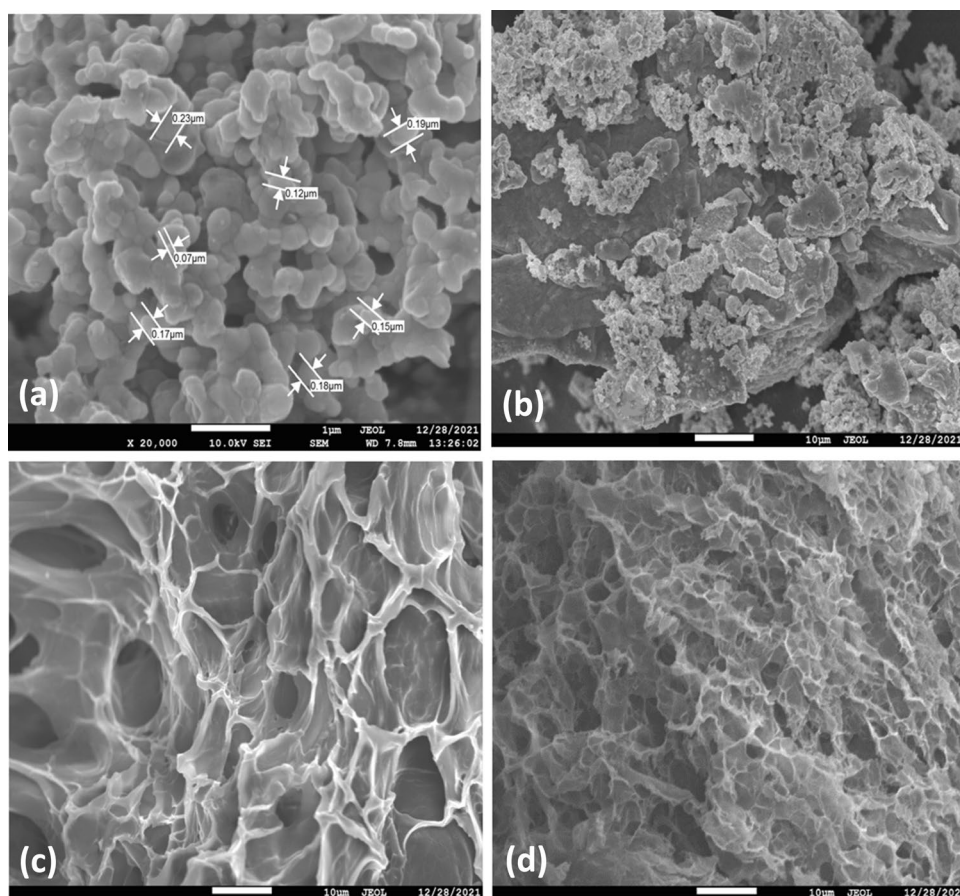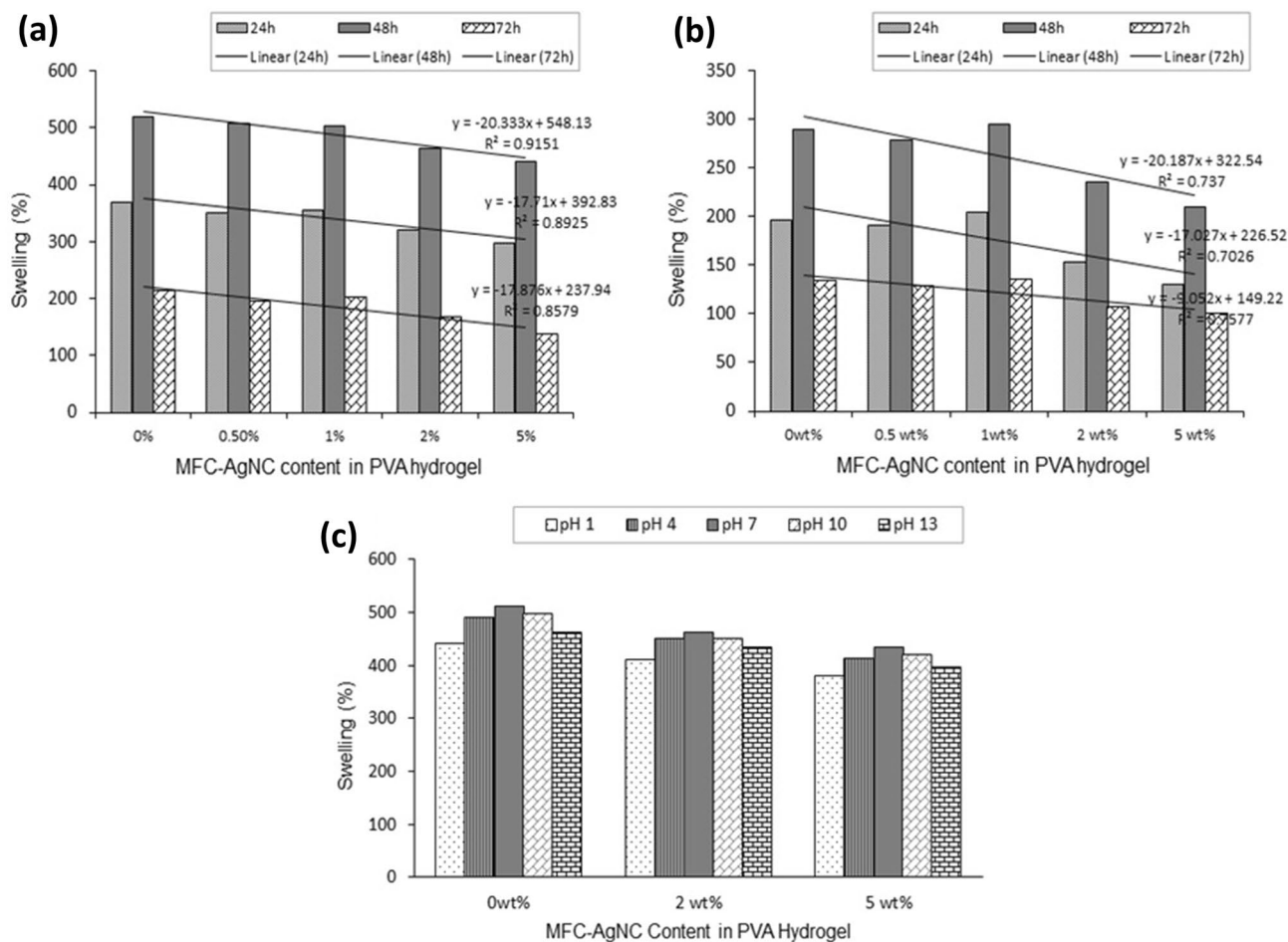
Fig. 6 Variation of swelling (%) of different PVA hydrogels in **a** distilled water, **b** NaCl (0.9%) solution with time 24 h, 48 h, 72 h and **c** solutions of pH 1, 4, 7, 10, 13 at 48 h

The DS of the hydrogel intensely dropped in the saline (0.9% NaCl) water compared to distilled water. Moreover, the DS of hydrogel in saline water decreased after 1 wt% of (MFC-Ag)NC loading i.e. the hydrogel with 1 wt% (MFC-Ag)NC showed maximum DS capacity in the saline water. Outwardly, the degree of cross-linking in the hydrogel is influenced by the Na^+ cation of saline water. Ag present in MFC may prohibit the entrance of Na^+ ion to form crosslinking in hydrogel and hence DS increases. At a very higher percentage of (MFC-Ag)NC, (MFC-Ag)NC itself forms a crosslinked network with PVA and borax hydrogel causing the reduction of DS and also from the SEM it was evident that the pore size decreased after the addition of (MFC-Ag)NC compared to the pure PVA hydrogel which in-turn decreased the swelling degree to a continuous manner. The maximum DS of hydrogel is also found at 48 h for saline water. More ionic density can reduce the gel stability which may act as the driving force for the breakdown of bonding between the PVA and (MFC-Ag)NC [52].

The DS of PVA hydrogel with 0 wt% (MFC-Ag)NC, 2 wt% (MFC-Ag)NC, and 5 wt% (MFC-Ag)NC was measured after 48 h in different pH solutions ranging from 1 to 13 to determine the sensitivity of the hydrogel samples. As expected, the maximum DS value was obtained at pH 7 for all types of samples and all samples showed a downward trend in DS with the incorporation of (MFC-Ag)NC. Furthermore, the DS decreased in both acidic and basic solutions. At lower pH, the alcoholic groups of PVA and carboxylic acid groups of (MFC-Ag)NC are protonated which can minimize the swelling proportion because of the reduction of anion-anion repulsion. In distilled water, the groups converted into ions of alcohol and carboxylate that resulting in the maximum repulsive electrostatic forces which in turn increased the DS of the hydrogel. However, in the basic solution, the alcohol and carboxylic groups changed to negatively charged ions which caused greater repulsion and expected to have more swelling in the hydrogels, we observed a decreased order. The possible reason is the presence of Ag^+ and Na^+ ions which diminished the formation

of negative carboxylate ions and hindered the effective electrostatic repulsion [53].
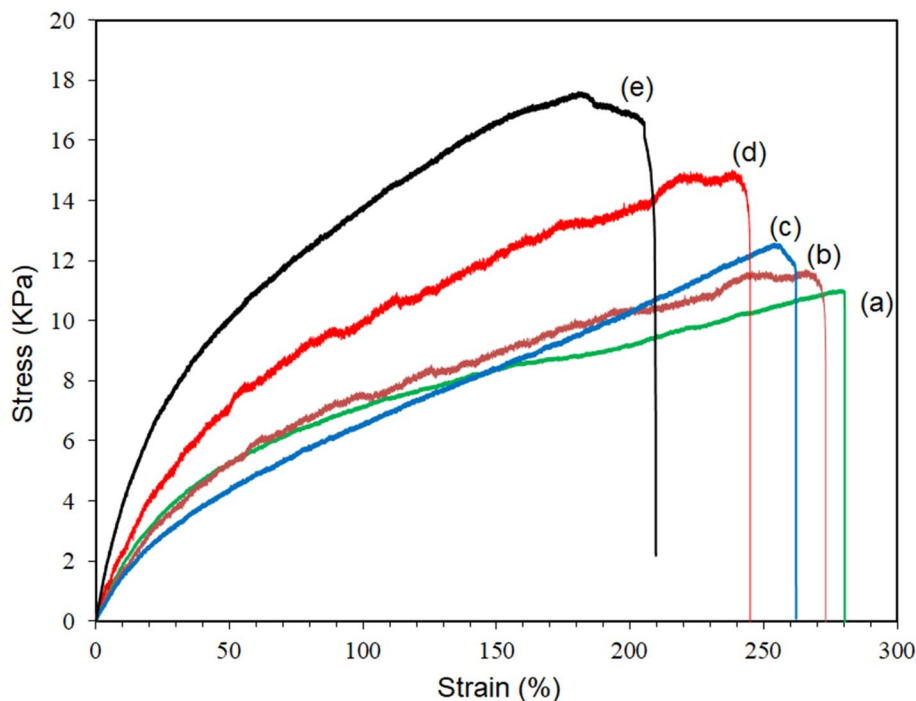
Tensile Properties

The summary of mechanical properties of a series of hydrogels including tensile strength, Young's modulus, and elongation at break with different (MFC-Ag)NC contents is listed in Table 1. The mechanical properties of (MFC-Ag)NC/PVA hydrogels were evaluated by uniaxial tensile measurements. The hydrogels with 0–5 wt% of (MFC-Ag)NC loading would lead to an increase in modulus and tensile strength. In (MFC-Ag)NC/PVA hydrogels, both covalent bonds and physical interactions between (MFC-Ag)NC and PVA chains might be stronger which led to the increase of tensile strength. This enhancement in mechanical behaviours would be related to the ability of (MFC-Ag)NC to change the energy dissipation process. Besides, the addition of a

small fraction of (MFC-Ag)NC led to a significant increase in Young's modulus (toughness). The moduli values are significantly higher than those reported by Han and co-workers [54], 0.9 kPa was reported for pure PVA-borax hydrogels and values ranging from 3.8 to 22.5 kPa was notified for gels reinforced with cellulose nanoparticles (Fig. 7).

This enhancement in mechanical properties can be attributed to the reinforcing influence of (MFC-Ag)NC. Liu et al. described the possible formation of a semi-interpenetrating network between nano-cellulose and PVA [55]. The strong interfacial interactions between the (MFC-Ag)NC and PVA impart restrictions on segments of the polymer chain during deformation leading to enhanced stiffness and strength. Entangled segments of nanocomposite act as a physical crosslinking agent, working in association with borax complexes towards maintaining the mechanical integrity of the hydrogels. This is supported by the increased gel content observed at (MFC-Ag)NC concentrations up to 5 wt%. At low degrees of crosslinking, polymer chains exhibit greater flexibility and freedom to move, increasing the possibility of bond reformation across the broken interface. Therefore elongation at break was found the highest in 0 wt% of (MFC-Ag)NC loading.

Thermogravimetric Properties

Figure 8 shows the TGA and DTG curves of (MFC-Ag)NC and PVA hydrogels with various (MFC-Ag)NC contents. The TGA curve of (MFC-Ag)NC indicates higher stability toward thermal degradation. From 30 to 600 °C, weight

Table 1 Tensile properties of hydrogels with different PVA/(MFC-Ag)NC loading

PVA hydrogel with (MFC-Ag)NC	Tensile strength (KPa)	Elongation (%)	Young modulus (KPa)
0wt%	10.8 ± 1.4	280.9 ± 4.2	5.4 ± 1.1
0.5wt %	11.5 ± 1.7	273.2 ± 2.9	6.9 ± 1.1
1wt %	12.1 ± 1.2	261.5 ± 3.3	8.4 ± 1.1
2wt%	14.5 ± 2.1	245.3 ± 3.3	12.7 ± 2.5
5wt%	16.3 ± 4.3	209.1 ± 1.3	23.9 ± 1.7

Fig. 7 Tensile stress–strain curves of **a** PVA hydrogel, **b** PVA/(MFC-Ag)NC (0.5wt%) hydrogel **c** PVA/(MFC-Ag)NC (1wt%) hydrogel, **d** PVA/(MFC-Ag)NC (2wt%) hydrogel, **e** PVA/(MFC-Ag)NC (5wt%) hydrogel
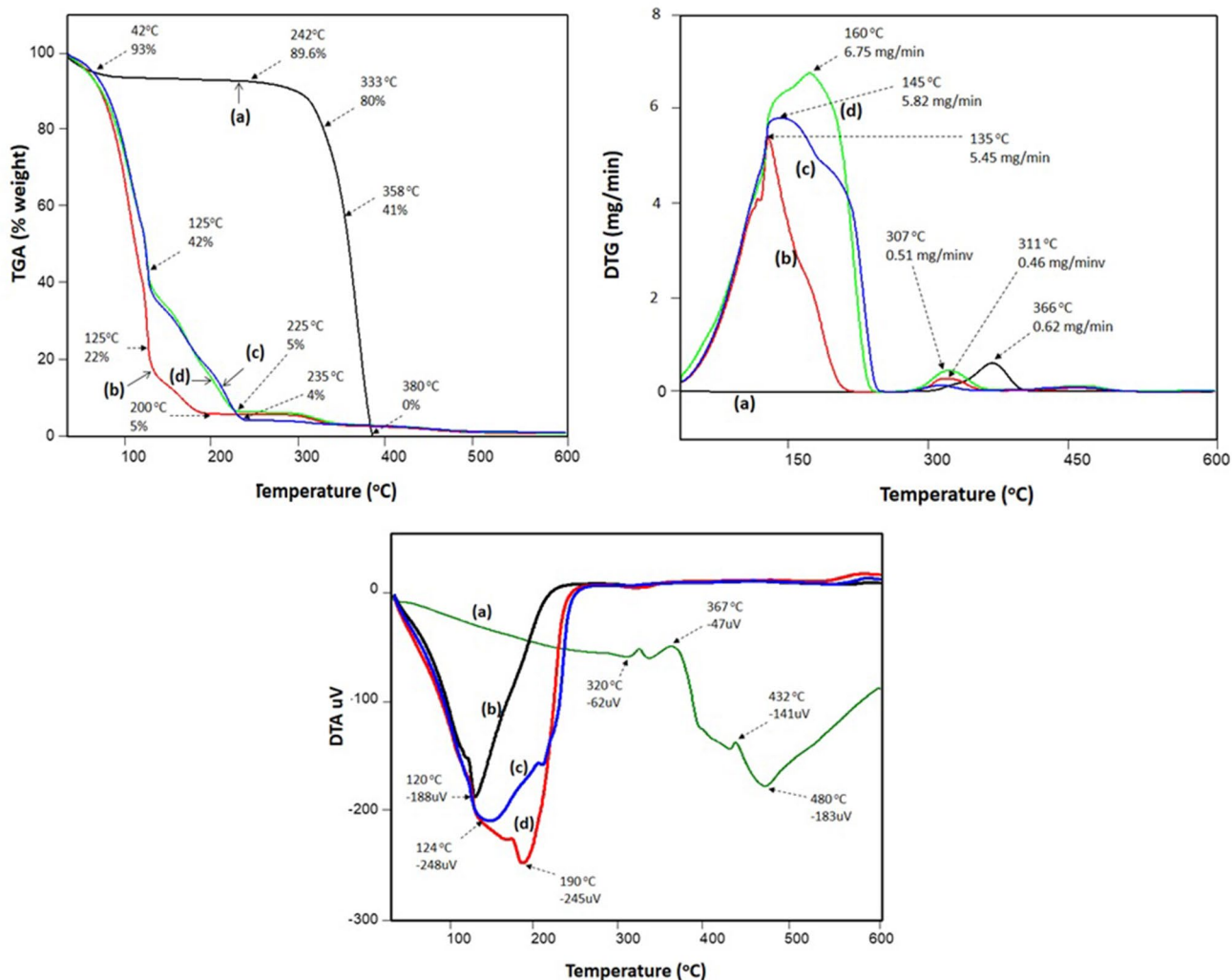
Fig. 8 TGA, DTG, and DTA curves of **a** (MFC-Ag)NC, **b** PVA hydrogels, **c** PVA hydrogel with 2wt% of (MFC-Ag)NC, **d** PVA hydrogel with 5wt% of (MFC-Ag)NC

loss percent of nanocomposite was observed and maximum degradation was observed from 242 to 380 °C. The TGA of (MFC-Ag)NC exhibited that the water content was approximately 7 wt%, and at 242–380 °C, 90% weight was lost which may be due to the degradation of the cellulose chain. PVA hydrogels with different percentages of (MFC-Ag)NC showed multiple steps of weight loss. The first steep weight loss started at 93 °C and is attributed to the loss of water in the sample which led to 60–80% weight loss till 125 °C in this stage. 2 wt% and 5 wt% (MFC-Ag) NC loaded hydrogels showed lower weight loss compared to pure PVA hydrogel. This is evidence of the semi-interpenetrating network formation between PVA hydrogel and (MFC-Ag)NC. The strong electrostatic forces between (MFC-Ag)NC and PVA molecules offer obstruction during degradation of the polymer chains and lead to improved

properties against thermal degradation. This data is also supported by a study performed by Sriupayo et al.[56]. The second step of degradation occurred at the temperature range from 135 to 225 °C. PVA started to degrade at around 130 °C. During degradation of PVA, the remaining water of gel is readily separated via vapor formation. The DTG graph shows the final degradation peaks at 366, 311, 307 and 303 °C for (MFC-Ag)NC, 0 wt% (MFC-Ag)NC/ PVA, 2 wt% (MFC-Ag)NC/PVA, 5 wt% (MFC-Ag)NC/ PVA hydrogels, respectively and the corresponding weight loss is 0.62 mg/min, 0.46 mg/min, 0.51 mg/min, 0.22 mg/ min. The DTA curve shows the endothermic peaks are located at around 120, 124, and 190 oC (Fig. 8) for 0 wt% (MFC-Ag)NC/PVA, 2 wt% (MFC-Ag)NC/PVA, 5 wt% (MFC-Ag)NC/PVA hydrogels, which fit well with the first step weight losses in the TG curve.
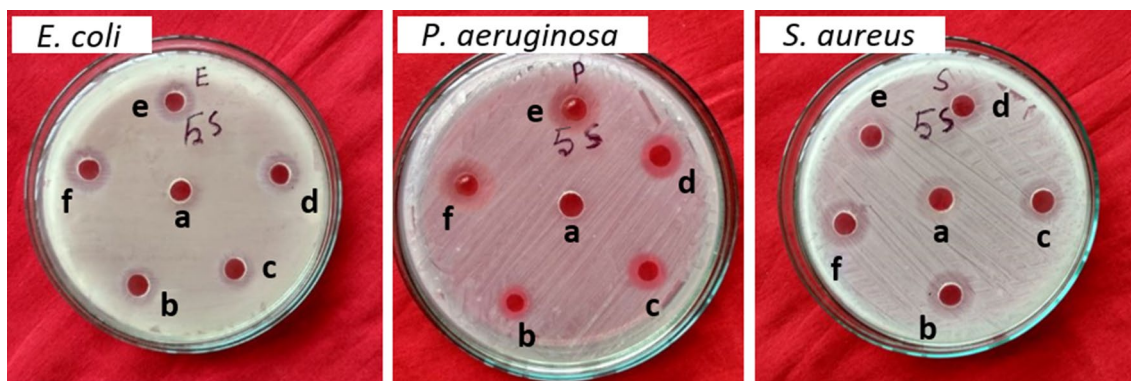
Fig. 9 Antimicrobial activities of **a** 0% (pure PVA), **b** 0.5%, **c** 1%, **d** 2%, **e** 5% (MFC-Ag)NC/PVA hydrogels, and **f** (MFC-Ag)NC against *E. coli*, *P. aeruginosa* and *S. aureus*

Table 2 Antimicrobial activity data of PVA hydrogels with different wt% of (MFC-Ag)NC against *E. coli*, *P. aeruginosa*, and *S. aureus*

Tested Microorganisms	Zone of Inhibition of study compound (mm)					
	PVA hydrogel with (MFC-Ag)NC					(MFC-Ag)NC
	0wt%	0.5wt%	1wt%	2wt%	5wt%	
Escherichia coli	×	1.0 ± 0.1	1.1 ± 0.1	1.9 ± 0.1	4.1 ± 0.2	4.5 ± 0.3
Pseudomonas aeruginosa	×	1.1 ± 0.3	1.5 ± 0.3	2.0 ± 0.2	4.5 ± 0.4	5.0 ± 0.5
Staphylococcus aureus	0.7 ± 0.1	1.8 ± 0.1	2.0 ± 0.1	2.3 ± 0.5	3.1 ± 0.4	3.9 ± 0.5

Anti-Microbial Activity

The antimicrobial activity of the hydrogel was observed against multi-drug resistant *E. coli* MZ20 (gram-negative), *P. aeruginosa* MZ2F (gram-negative), and *S. aureus* MZ18 (gram-positive) through the agar well diffusion method. As shown in Fig. 9, the pure PVA hydrogel does not show any antibacterial activity. (MFC-Ag)NC/PVA hydrogels showed that the antibacterial ability increased with an increasing percentage of (MFC-Ag)NC. With the addition of (MFC-Ag)NC to the culture medium, it was expected to get attached to the cell wall of the bactericides and because of the nature of Ag nanoparticles, it destroyed the cell walls and affected the protein and other cellular components leakage and at last killed the cells. Ag nanoparticles can rapidly degenerate to form free radicals by redox reaction. During the reaction, Ag^+ ion is formed which is responsible for the formation of reactive oxygen species (ROS) resulting the oxidative stress. Studies showed that nanoparticles can increase the level of ROS up to 50 fold. When the cells of gram-positive and gram-negative bacteria experience oxidative stress, a series of dysfunctions are observed in their lipid membrane, protein and DNA which stop cell growth and destroy them [57, 58].

Table 2 shows that the antimicrobial efficiency of (MFC-Ag)NC/PVA hydrogel depended on the concentration of the (MFC-Ag)NC regardless of the form of bacteria used. That's why the best antibacterial effect was observed by (MFC-Ag)NC only. It is clear that, with a higher percentage of (MFC-Ag)NC content, the hydrogel samples exhibited an extended inhibition zone around the wells. 5% (MFC-Ag)NC/PVA hydrogels showed the maximum antimicrobial action against *E. coli*, *P. aeruginosa,* and *S. aureus*. The maximum width of the zone of inhibition of (MFC-Ag)NC/PVA hydrogels against *E. coli*, *P. aeruginosa,* and *S. aureus* were 4.1 ± 0.2, 4.5 ± 0.4, and 3.1 ± 0.4 mm respectively. By analyzing the outcomes we can also discover that (MFC-Ag)NC hydrogels exhibited better activity against gram-negative bacteria compared to gram-positive bacteria.

Conclusions

A novel hydrogel has been prepared using micro-fibrillated cellulose embedded silver nanocomposite and PVA, using borax as a crosslinking agent to improve the gel strength and antibacterial properties. The process for the preparation of nanocomposite and hydrogel is eco-friendly and inexpensive. The details of the structure were studied by UV–vis

spectroscopy, XRD investigation, FTIR spectroscopy, and SEM which supported the formation of nanocomposite and hydrogel. Furthermore, the swelling property of the gel is dependent on time, salt present, pH, and weight fraction of (MFC-Ag)NC in PVA hydrogel. The degree of swelling was found the highest in distilled water at pH 7.0 because of the strong anion-anion repulsion and its value is decreased with the increases of the percent of (MFC-Ag)NC. Tensile strength and modulus of hydrogels were increased with the addition of a different percentage of (MFC-Ag)NC whereas elongation percentage showed the reverse trend. The weight loss percentage and rate of degradation have been determined through thermogravimetry. The initial weight loss due to bound water of hydrogel was found the highest for pure PVA hydrogel which decreased with the increasing percentage of (MFC-Ag)NC. The presence of (MFC-Ag)NC in PVA gels aided effective microbial penetration and the samples containing silver expressed antimicrobial activity against both gram-negative (*E. coli, P. aeruginosa*) and gram-positive (*S. aureus*) bacteria although the effectiveness was better against both the gram-negative bacteria than the gram-positive bacteria. Based on the observed results, PVA hydrogels with (MFC-Ag)NC can therefore be used in a controlled release system and also can be considered as a potential platform for further development of antibacterial wound dressing.

Declarations

Conflict of interest The authors declare not to have any conflict of interest.

References

1. Yahia Lh (2015) History and applications of hydrogels. J Biomed Sci 04(02):1–23. https://doi.org/10.4172/2254-609X.100013
2. Yang J, Gong C, Shi FK, Xie XM (2012) High strength of physical hydrogels based on poly(acrylic acid)-g-poly(ethylene glycol) methyl ether: Role of chain architecture on hydrogel properties. J Phys Chem B 116(39):12038–12047. https://doi.org/10.1021/jp303710d
3. García-Astrain C et al (2015) Biocompatible hydrogel nanocomposite with covalently embedded silver nanoparticles. Biomacromol 16(4):1301–1310. https://doi.org/10.1021/acs.biomac.5b00101
4. Thoniyot P, Tan MJ, Karim AA, Young DJ, Loh XJ (2015) Nanoparticle–hydrogel composites: concept, design, and applications of these promising, multi-functional materials. Adv Sci 2(1–2):1–13. https://doi.org/10.1002/advs.201400010
5. Ahmed EM (2015) Hydrogel: Preparation, characterization, and applications: A review. J Adv Res 6(2):105–121. https://doi.org/10.1016/j.jare.2013.07.006
6. Oliveira RN et al (2013) Mechanical properties and in vitro characterization of polyvinyl alcohol-nano-silver hydrogel wound dressings. Interface Focus 4(1):20130049–20130049. https://doi.org/10.1098/rsfs.2013.0049
7. Raho R et al (2020) Photo-assisted green synthesis of silver doped silk fibroin/carboxymethyl cellulose nanocomposite hydrogels for biomedical applications. Mater Sci Eng C. https://doi.org/10.1016/j.msec.2019.110219
8. Zhang H, Xia H, Zhao Y (2012) Poly (vinyl alcohol) hydrogel can autonomously self-heal. ACS Macro Lett. https://doi.org/10.1021/mz300451r
9. Hassan CM, Peppas NA (2000) Structure and applications of poly(vinyl alcohol) hydrogels produced by conventional crosslinking or by freezing/thawing methods. Biopolym PVA Hydrogels, Anionic Polym Nanocomposites 153:37–65. https://doi.org/10.1007/3-540-46414-X_2
10. Anjum S, Sharma A, Tummalapalli M, Joy J, Bhan S, Gupta B (2015) A novel route for the preparation of silver loaded polyvinyl alcohol nanogels for wound care systems. Int J Polym Mater Polym Biomater 64(17):894–905. https://doi.org/10.1080/00914037.2015.1030660
11. Lu B et al (2017) One-pot assembly of microfibrillated cellulose reinforced PVA-borax hydrogels with self-healing and ph-responsive properties. ACS Sustain Chem Eng 5(1):948–956. https://doi.org/10.1021/acssuschemeng.6b02279
12. Sinton SW (1987) Complexation chemistry of sodium borate with poly(vinyl alcohol) and small diols: A11B NMR study. Macromolecules 20(10):2430–2441. https://doi.org/10.1021/ma00176a018
13. Sczostak A (2009) Cotton linters: An alternative cellulosic raw material. Macromol Symp 280(1):45–53. https://doi.org/10.1002/masy.200950606
14. Lin HL, Liu YF, Yu TL, Liu WH, Rwei SP (2005) Light scattering and viscoelasticity study of poly(vinyl alcohol)-borax aqueous solutions and gels. Polymer (Guildf) 46(15):5541–5549. https://doi.org/10.1016/j.polymer.2005.04.074
15. Zhang F, Wu J, Kang D, Zhang H (2013) Development of a complex hydrogel of hyaluronan and PVA embedded with silver nanoparticles and its facile studies on Escherichia coli. J Biomater Sci Polym Ed 24(12):1410–1425. https://doi.org/10.1080/09205063.2012.763109
16. Sirousazar ZMHM, Kokabi M (2011) Swelling behavior and structural characteristics of polyvinyl alcohol/montmorillonite nanocomposite hydrogels. J Appl Polym Sci 123:50–58. https://doi.org/10.1002/app
17. Rai M, Yadav A, Gade A (2009) Silver nanoparticles as a new generation of antimicrobials. Biotechnol Adv 27(1):76–83. https://doi.org/10.1016/j.biotechadv.2008.09.002
18. Fu LH, Liu B, Meng LY, Ma MG (2016) Comparative study of cellulose/Ag nanocomposites using four cellulose types. Mater Lett 171:277–280. https://doi.org/10.1016/j.matlet.2016.02.118
19. P. Mohamadinia, "Preparation And Characterization of Sodium Alginate / Acrylic Acid Composite Hydrogels Conjugated To Silver Nanoparticles As An Antibiotic Delivery System," *Res. Sq.*, pp. 1–13, 2021, [Online]. Available: https://www.researchsquare.com/article/rs-429387/v1.
20. Song S et al (2021) Antibacterial polyvinyl alcohol/bacterial cellulose/nano-silver hydrogels that effectively promote wound healing. Mater Sci Eng C 126:112171. https://doi.org/10.1016/j.msec.2021.112171
21. Wang L, Periyasami G, Aldalbahi A, Fogliano V (2021) The antimicrobial activity of silver nanoparticles biocomposite

films depends on the silver ions release behaviour. Food Chem 359:129859. https://doi.org/10.1016/j.foodchem.2021.129859

22. Abbate F, Santos D, Iulianelli GCV, Inês M, Tavares B (2016) The use of cellulose nanofillers in obtaining polymer nanocomposites: properties, processing, and applications. Mater Sci Appl 7(7):257–294. https://doi.org/10.4236/msa.2016.75026

23. Siró I, Plackett D (2010) Microfibrillated cellulose and new nanocomposite materials: A review. Cellulose 17(3):459–494. https://doi.org/10.1007/s10570-010-9405-y

24. Ovalle-Serrano SA, Díaz-Serrano LA, Hong C, Hinestroza JP, Blanco-Tirado C, Combariza MY (2020) Synthesis of cellulose nanofiber hydrogels from fique tow and Ag nanoparticles. Cellulose 27(17):9947–9961. https://doi.org/10.1007/s10570-020-03527-6

25. M. F. Rosa *et al.*, "EXTRAÇÃO E CARACTERIZAÇÃO DE 'WHISKERS' DE CELULOSE DE FIBRA DE COCO," *Congr. Bras. Eng. e Ciência dos Mater.*, pp. 4050–4058, 2008, [Online]. Available: https://www.alice.cnptia.embrapa.br/alice/bitstream/doc/28217/1/Proci08.00139.pdf.

26. Shin JU, Gwon J, Lee SY, Yoo HS (2018) Silver-incorporated nanocellulose fibers for antibacterial hydrogels. ACS Omega 3(11):16150–16157. https://doi.org/10.1021/acsomega.8b02180

27. Sharma VK, Yngard RA, Lin Y (2009) Silver nanoparticles: Green synthesis and their antimicrobial activities. Adv Colloid Interface Sci 145(1–2):83–96. https://doi.org/10.1016/j.cis.2008.09.002

28. Yang KK, Wang XL, Wang YZ (2007) Progress in nanocomposite of biodegradable polymer. J Ind Eng Chem 13(4):485–500

29. Cobos M, De-La-Pinta I, Quindós G, Fernández MJ, Fernández MD (2020) alcohol) / graphene oxide – silver nanoparticles. Polymers (Basel) 12(723):1–18

30. Fan L, Zhang H, Gao M, Zhang M, Liu P, Liu X (2019) Cellulose nanocrystals/silver nanoparticles: In-situ preparation and application in PVA films. Holzforschung 74(5):523–528. https://doi.org/10.1515/hf-2018-0251

31. Sarwar MS, Niazi MBK, Jahan Z, Ahmad T, Hussain A (2018) Preparation and characterization of PVA/nanocellulose/Ag nanocomposite films for antimicrobial food packaging. Carbohydr Polym 184:453–464. https://doi.org/10.1016/j.carbpol.2017.12.068

32. Nain Z, Islam MA, Minnatul Karim M (2019) Antibiotic resistance profiling and molecular phylogeny of biofilm forming bacteria from clinical and non-clinical environment in southern part of Bangladesh". Int J Enteric Pathog. https://doi.org/10.15171/ijep.2019.10

33. Rahman M, Khan G, Uddin M, Razzaque S, Alam M (2016) Chemical treatments of cotton linter cellulose fiber for composite application. Am Chem Sci J 16(4):1–7. https://doi.org/10.9734/acsj/2016/28730

34. Gomes A, Goda K, Ohgi J (2004) Effects of alkali treatment to reinforcement on tensile properties of Curaua fiber green composites. JSME Int Journal Ser A Solid Mech Mater Eng. https://doi.org/10.1299/jsmea.47.541

35. Butterworth E (1939) The bleaching of cellulose, with special reference to bast fibres. J Soc Dyers Colour 55(12):589–596

36. Li W, Wang R, Liu S (2011) Nanocrystalline cellulose prepared from softwood kraft pulp via ultrasonic-assisted acid hydrolysis. BioResources 6(4):4271–4281. https://doi.org/10.15376/biores.6.4.4271-4281

37. G. M. A. Khan *et al.*, "Mechanical, thermal and morphological studies of microfibrillated jute/PLA biocomposites," *Indian J Fibre Text Res*, vol. 42, no. 3, 2017.

38. Priya SY, Khan GMA, Uddin MH, Haque MA, Islam MS, Gafur MA (2015) Characterization of micro-fibrillated cellulose produced from sawmill wastage: crystallinity and thermal properties.

Am Chem Sci J 9(1):1–8. https://doi.org/10.9734/ACSj/2015/19752

39. Spoljaric S, Salminen A, Luong ND, Seppälä J (2014) Stable, self-healing hydrogels from nanofibrillated cellulose, poly(vinyl alcohol) and borax via reversible crosslinking. Eur Polym J 56(1):105–117. https://doi.org/10.1016/j.eurpolymj.2014.03.009

40. Magaldi S et al (2004) Well diffusion for antifungal susceptibility testing. Int J Infect Dis 8(1):39–45. https://doi.org/10.1016/j.ijid.2003.03.002

41. National Committee for Clinical Laboratory Standards, *Performance Standards for Antimicrobial Disk Susceptibility Tests*, Fifth Edit. Villanova, PA, USA: Approved Standard NCCLS Publication M2-A5, 1993.

42. Al Masud MA et al (2021) Green synthesis of silk sericin-embedded silver nanoparticles and their antibacterial application against multidrug-resistant pathogens. J Genet Eng Biotechnol. https://doi.org/10.1186/s43141-021-00176-5

43. Zhang X, Sun H, Tan S, Gao J, Fu Y, Liu Z (2019) Hydrothermal synthesis of Ag nanoparticles on the nanocellulose and their antibacterial study. Inorg Chem Commun 100:44–50. https://doi.org/10.1016/j.inoche.2018.12.012

44. Biao L et al (2017) Synthesis, characterization and antibacterial study on the chitosan-functionalized Ag nanoparticles. Mater Sci Eng C 76:73–80. https://doi.org/10.1016/j.msec.2017.02.154

45. Kwon G-J et al (2020) Adsorption characteristics of Ag nanoparticles on cellulose nanofibrils with different chemical compositions. Polymers (Basel) 12(1):164. https://doi.org/10.3390/polym12010164

46. Suflet DM, Chitanu GC, Popa VI (2006) Phosphorylation of polysaccharides: New results on synthesis and characterisation of phosphorylated cellulose. React Funct Polym 66(11):1240–1249. https://doi.org/10.1016/j.reactfunctpolym.2006.03.006

47. Uesu NY, Pineda EAG, Hechenleitner AAW (2000) Microcrystalline cellulose from soybean husk: effects of solvent treatments on its properties as acetylsalicylic acid carrier. Int J Pharm 206(1–2):85–96. https://doi.org/10.1016/S0378-5173(00)00532-9

48. Alemdar A, Sain M (2008) Isolation and characterization of nanofibers from agricultural residues - Wheat straw and soy hulls. Bioresour Technol 99(6):1664–1671. https://doi.org/10.1016/j.biortech.2007.04.029

49. Kobayashi M, Kitaoka Y, Kobayashi M (1997) Complex formation of boric acids with DI-and TRI-carboxylic acids and poly (vinyl alcohol) in aqueous solutions. Macromol Symp 114(1):303–308

50. Cui XF et al (2019) Water-retaining, tough and self-healing hydrogels and their uses as fire-resistant materials. Polym Chem 10(37):5151–5158. https://doi.org/10.1039/C9PY01015G

51. Shenoy SL, Painter PC, Coleman MM (1999) The swelling and collapse of hydrogen bonded polymer gels. Polymer (Guildf) 40(17):4853–4863. https://doi.org/10.1016/S0032-3861(98)00699-5

52. Wang D, Zhao S, Yin R, Li L, Lou Z, Shen G (2021) "Recent advanced applications of ion-gel in ionic-gated transistor", *npj Flex. Electron* 5(1):13. https://doi.org/10.1038/s41528-021-00110-2

53. Namazi H, Hasani M, Yadollahi M (2019) Antibacterial oxidized starch/ZnO nanocomposite hydrogel: synthesis and evaluation of its swelling behaviours in various pHs and salt solutions. Int J Biol Macromol 126:578–584

54. Han J, Lei T, Wu Q (2013) Facile preparation of mouldable polyvinyl alcohol-borax hydrogels reinforced by well-dispersed cellulose nanoparticles: physical, viscoelastic and mechanical properties. Cellulose 20(6):2947–2958

55. Liu J, Li Q, Su Y, Yue Q, Gao B, Wang R (2013) Synthesis of wheat straw cellulose-g-poly (potassium acrylate)/PVA semi-IPNs superabsorbent resin. Carbohydr Polym 94(1):539–546

56. Sriupayo J, Supaphol P, Blackwell J, Rujiravanit R (2005) Preparation and characterization of α-chitin whisker-reinforced chitosan nanocomposite films with or without heat treatment. Carbohydr Polym 62(2):130–136. https://doi.org/10.1016/j.carbpol.2005.07.013

57. Davies KJA (2000) Oxidative stress, antioxidant defenses, and damage removal, repair, and replacement systems. IUBMB Life 50(4–5):279–289

58. Quinteros MA, Aristizábal VC, Dalmasso PR, Paraje MG, Páez PL (2016) Oxidative stress generation of silver nanoparticles in three bacterial genera and its relationship with the antimicrobial activity. Toxicol Vitr 36:216–223

Publisher's Note Springer Nature remains neutral with regard to jurisdictional claims in published maps and institutional affiliations.

Authors and Affiliations

Md. Sabbir Hasan[1,2] · Jannat Al Foisal[1,4] · G. M. Arifuzzaman Khan[1] · Rownok Jahan[1] · Md. Hasanuzzaman[1,6] · Md. Shamsul Alam[1] · M. Minnatul Karim[3] · M. A. Gafur[5] · Muhammad Angkan Khan[3] · Md. Abdus Sabur[3]

✉ Md. Shamsul Alam
dr.alamiu@yahoo.com

[1] Department of Applied Chemistry and Chemical Engineering, Faculty of Engineering and Technology, Islamic University, Kushtia 7003, Bangladesh

[2] BCSIR Laboratories Rajshahi, Bangladesh Council of Scientific and Industrial Research, Rajshahi 6206, Bangladesh

[3] Department of Biotechnology and Genetic Engineering, Islamic University, Kushtia 7003, Bangladesh

[4] Department of General Educational Development, Daffodil International University, Dhaka, Bangladesh

[5] PP and PDC, Bangladesh Council of Scientific and Industrial Research, Dhaka 1205, Bangladesh

[6] Institute of Glass and Ceramic Research & Testing, Bangladesh Council of Scientific and Industrial Research, Dhaka 1205, Bangladesh